PROCEEDINGS OF THE ROYAL SOCIETY A MATHEMATICAL, PHYSICAL & ENGINEERING SCIENCES

A computational framework for agglomeration in thermochemically reacting granular flows

T. I. Zohdi

Proc. R. Soc. Lond. A 2004 **460**, 3421-3445
doi: 10.1098/rspa.2004.1277

10.1098/rspa.2004.1277

THE ROYAL SOCIETY

A computational framework for agglomeration in thermochemically reacting granular flows

By T. I. Zohdi

Department of Mechanical Engineering, 6195 Etcheverry Hall, University of California, Berkeley, CA 94720-1740, USA (zohdi@newton.berkeley.edu)

Received 15 March 2003; accepted 13 January 2004; published online 25 August 2004

A computational framework is developed which couples a series of models, each describing vastly different physical events, in order to characterize particle growth (agglomeration) in thermochemically reacting granular flows. The modelling is purposely simplified to expose the dominant mechanisms which control agglomeration. The overall system is comprised of relatively simple coupled submodels describing impact, heat production, bonding and fragmentation, each of which can be replaced by more elaborate descriptions, if and when they are available. Inverse problems, solved with a genetic algorithm, are then constructed to ascertain system parameters which maximize agglomeration likelihood within a range of admissible data.

Keywords: granular flows; thermochemical coupling; agglomeration

1. Introduction

This work focuses on the development of a computational framework to simulate granular particulate growth, 'agglomeration', in thermochemically reacting environments. Applications arise in the study of interstellar granular dust flows in the presence of dilute hydrogen-rich gas. In the description of dust collisions and growth in gaseous protoplanetary accretion discs, one school of thought is that grains collide, adhere and grow into larger objects, usually referred to as protoplanets. For investigations on various aspects of this complex phenomenon, see Du *et al*. (1995), Kokubo & Ida (2000, 1996), Grazier *et al*. (2000, 1999), Supulver & Lin (2000), Tanga *et al*. (1996), Cuzzi *et al*. (1993), Weidenschilling & Cuzzi (1993), Weidenschilling *et al*. (1997), Beckwith *et al*. (2000), Barge & Sommeria (1995), Lissauer (1993), Barranco *et al*. (2001), Barranco & Marcus (2001), Benz (2000, 1994), Blum & Wurm (2000), Dominik & Tielens (1997), Chokshi *et al*. (1993) and Wurm *et al*. (2001).

Usually, due to the complexity of this class of problems, at the simulation level, most analyses concentrate only on one aspect of the series of events that occur in such granular flows. Since modelling of these coupled events is rather complicated, and there being no overall framework available which could be used as a basis, the present work aims to provide this larger perspective on the problem. The modelling is purposely simplified to expose the dominant phenomenological controlling agglomeration mechanisms, and their coupled interaction.† The overall system is

† Throughout the analysis, we shall highlight the limitations and deficiencies of such models.

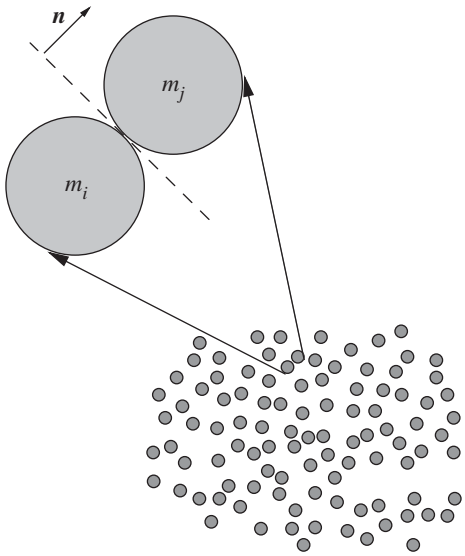

Figure 1. The impact of two particles in a granular flow.

comprised of relatively simple submodels describing impact, thermochemical heat production, bonding and fragmentation, each of which can be replaced by more elaborate descriptions, if and when they are available. Impact parameters, such as the coefficient of restitution, play a central role in any granular flow analysis. Such parameters are functions of the pressure and temperature, which implicitly depend on, among other things, the relative velocity of the contact surfaces of the particles. Generally, all of the preceding quantities are unknown *a priori*, since they depend on the state variables. For systems of impacting particles, this leads to an enormous number of coupled nonlinear equations. The situation is complicated by the possibility that the fusing of particles, silicates for example, may occur in a reactive, gaseous hydrogen-rich environment. The high strain rates in such impact scenarios, coupled with thermochemical reactions due to reactive materials present on the surface of particles, may lead to significant thermal softening, and possibly a rapidly formed molten interparticle layer, which, upon cooling, strongly fuses the colliding pair together. These effects greatly enhance bonding. In this work, a temporally adaptive multilevel staggering scheme is developed to solve the system of nonlinear equations that arise from the coupled model. Thereafter, inverse problems for parameter identification are constructed whereby transient flow conditions, reaction rates, particulate volume fractions, hardnesses, etc., are sought to maximize the likelihood of larger particles forming (agglomeration) within a range of admissible data. A statistical genetic algorithm is developed to solve the non-convex and non-differentiable inverse problem, and three-dimensional numerical examples are given to illustrate the behaviour of the model and the overall solution process.

2. Momentum exchange

A class of model problems is considered that consists of a cloud of randomly distributed grains with initial velocities that are randomly perturbed around a mean value (figure 1). *We treat the grains as spherical particles, i.e. their rotation with*

respect to their centres of mass is deemed insignificant.† For the sake of presentation clarity, we use a shifted time variable at the beginning of impact, time $t = t_0$, defined by $\tau = t - t_0$. For two colliding particles i and j, normal to the line of impact, we have a conservation of momentum, before ($\tau = 0$) and after ($\tau = \delta\tau$) impact (figure 1),

$$m_i v_{i\mathrm{n}}(0) + m_j v_{j\mathrm{n}}(0) = m_i v_{i\mathrm{n}}(\delta\tau) + m_j v_{j\mathrm{n}}(\delta\tau), \tag{2.1}$$

where the subscript 'n' denotes the normal component of the velocity (along the line connecting particle centres). If one isolates one of the members of the colliding pair, then

$$m_i v_{i\mathrm{n}}(0) + \bar{I}_{\mathrm{n}}\delta\tau = m_i v_{i\mathrm{n}}(\delta\tau) \quad \Rightarrow \quad \bar{I}_{\mathrm{n}} = \frac{m_i(v_{i\mathrm{n}}(\delta\tau) - v_{i\mathrm{n}}(0))}{\delta\tau}, \tag{2.2}$$

where $\bar{I}_{\mathrm{n}}$ is the average impulsive force acting during the impact event between the particles. In addition to momentum transfer, an auxiliary relation comes from the commonly used material parameter, the coefficient of restitution, defined by the ratio of the relative velocities before and after impact:

$$e \stackrel{\mathrm{def}}{=} \frac{v_{j\mathrm{n}}(\delta\tau) - v_{i\mathrm{n}}(\delta\tau)}{v_{i\mathrm{n}}(0) - v_{j\mathrm{n}}(0)}. \tag{2.3}$$

If e were explicitly known, then one could write

$$v_{i\mathrm{n}}(\delta\tau) = \frac{m_i v_{i\mathrm{n}}(0) + m_j(v_{j\mathrm{n}}(0) - e(v_{i\mathrm{n}}(0) - v_{j\mathrm{n}}(0)))}{m_i + m_j} \tag{2.4}$$

and

$$v_{j\mathrm{n}}(\delta\tau) = v_{i\mathrm{n}}(\delta\tau) + e(v_{i\mathrm{n}}(0) - v_{j\mathrm{n}}(0)). \tag{2.5}$$

Remarks 2.1. A primary simplifying assumption is made. *The particles, and any subsequent agglomerations of particles that are formed, are spherical before and after impact. Furthermore, the agglomerations are also considered to be particles.* Thus, during the calculations, if the value of $\|\boldsymbol{r}_i - \boldsymbol{r}_j\|$ is smaller than the sum of the two radii, then contact occurs, since the geometries of the particles and subsequent agglomerations are approximated as being spherical. The sizes of the agglomerations can be determined by their total mass,

$$\rho_i \tfrac{4}{3}\pi b_i^3 = n m_i \quad \Rightarrow \quad b_i = \left(\frac{n m_i}{\rho_i \frac{4}{3}\pi}\right)^{1/3},$$

where n is the total number of particles in an agglomeration.

3. Impact-dependent restitution coefficients

The phenomenological parameter e depends on the severity of the impact velocity and, implicitly, among other things, the pressure in the contact zone (see Goldsmith (2001) for extensive experimental data or Johnson (1987) for detailed analytical treatments). For the applications considered, involving particle bonding, leading to agglomeration in thermochemically reacting granular media, it is advantageous

† Henceforth, we use the term 'grain' and 'particle' interchangeably.

to construct coefficient of restitution relations that are pressure and temperature based, which idealize bonding as a limiting case as $e \to 0$. For example, development of ad hoc, empirically derived relations involving the material's Vicker's hardness and temperature to determine whether two particles bond can be found in Zohdi (2003*a*), and are based on empirical adhesion conditions developed in Nesterenko *et al.* (1994) (see Meyers (1994) or Nesterenko (2001) for reviews on such bonding criteria).

Specifically, the phenomenological material parameter e depends on $\bar{I}_{\rm n}$, and thus implicitly on the impact velocity. An empirically derived condition for whether two surfaces will bond is if the magnitude of the surface pressure (P) exceeds or attains twice the Vicker's hardness $2H$, i.e. if $|P| \geqslant 2H$ (see Meyers (1994), Nesterenko (2001) or Nesterenko *et al.* (1994) for reviews).† We construct an ad hoc model for bonding by approximating the surface pressure as $P \approx |\bar{I}_{\rm n}|/a^{\rm c}$, where $a^{\rm c}$ represents the apparent contact area. Clearly, if $e = 1$, the impact is purely elastic with no adhesion, and thus there is no loss in energy, while if $e = 0$ there is a maximum loss in energy. Consistent with Nesterenko's experimental observations on bonding (Nesterenko 2001; Nesterenko *et al.* 1994), we shall make the ad hoc assumption that if the pressure exceeds twice the Vicker's hardness, the two surfaces will bond. Furthermore, we approximate e by a linear scaling with the pressure to hardness ratio‡

$$e \stackrel{\rm def}{=} \frac{v_{j{\rm n}}(\delta\tau) - v_{i{\rm n}}(\delta\tau)}{v_{i{\rm n}}(0) - v_{j{\rm n}}(0)} \approx \max\left(1 - \frac{|\bar{I}_{\rm n}|/a^{\rm c}}{2H}, 0\right) = \max\left(1 - \frac{m_i|v_{i{\rm n}}(\delta\tau) - v_{i{\rm n}}(0)|}{2a^{\rm c}H\delta\tau}, 0\right). \tag{3.1}$$

Since e is a function of the post-impact velocity, via $\bar{I}_{\rm n} = \bar{I}_{\rm n}(\boldsymbol{v}(\delta\tau))$, equations (2.4), (2.5) and (3.1), along with relations that govern changes in other variables (contact area and friction), are strongly coupled. One approach to solve such a system, in fact the one adopted later in this work, is to employ a recursive (fixed-point type) staggering process, whereby one first assumes permanent adhesion $e = 0$, computing $v_{i{\rm n}}(\delta\tau)$ and $v_{j{\rm n}}(\delta\tau)$, then checks the implicit assumption of whether or not $|P| \geqslant 2H$ is correct. If $|P| < 2H$, then $e = 1 - (|\bar{I}_{\rm n}|/2a^{\rm c}H)$ and the velocities are recomputed. The procedure is repeated until the difference between successive solutions is below a given tolerance. Essentially, the same relations can be computed for all impacting pairs. This is elaborated upon further in the work.

Remarks 3.1. Clearly, several components of the model are based upon ad hoc assumptions and can be improved. For example, treatment of the grains as non-rotating spherical particles is only valid if their rotation with respect to their centres of mass is deemed insignificant. For fine-scale interstellar 'dust' the particulate approximation is reasonable; however, as the particles grow, it is not. The bonding criteria, constructed in an ad hoc manner from the experiments of Nesterenko *et al.* (1994), can be improved, in particular by considering subscale models which resolve the contact between particles in detail with an embedded, detailed analysis, via a finite-element calculation, for example. Furthermore, the rotation of the particles due to friction can then be taken into account, as well as the thermochemical effects

† The Vicker's hardness is correlated to the yield point for plastic deformation of the material by $H \approx 3\sigma_y$.

‡ If the two bodies have different hardnesses, the smaller of the two values is used.

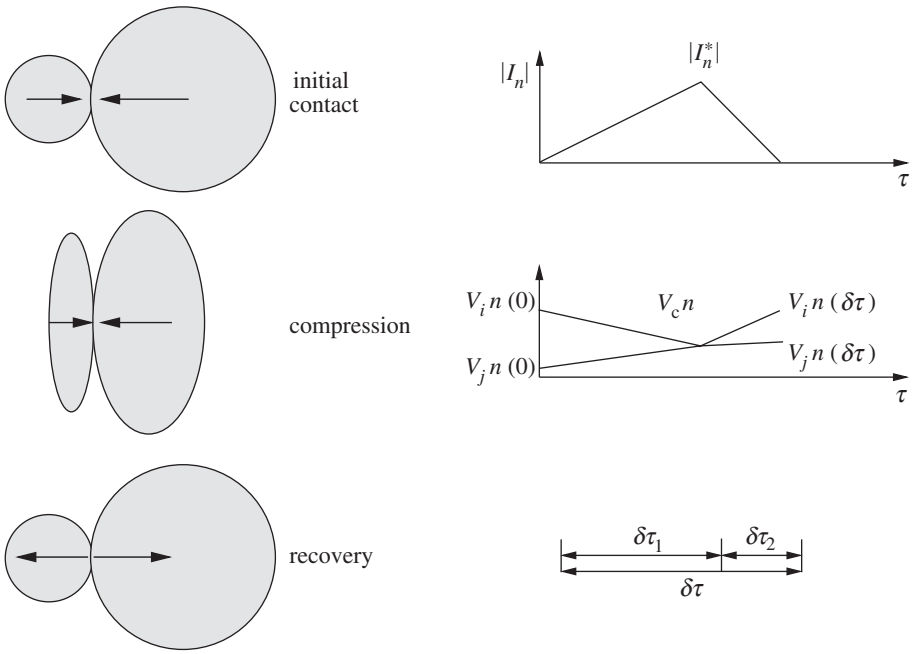

Figure 2. Compression and recovery of two impacting particles.

induced by contact. However, this is beyond the scope of the present analysis (see Wriggers (2002) for details). Also, the assumptions of self-similar growth (smaller spheres combining to form larger spheres) and, later in the analysis, self-similar fragmentation (larger spheres broken down into smaller spheres) are unrealistic. Such a model is used primarily to simplify the contact detection and post-impact fragmentation. Clearly, the objects in the flow will fragment into irregular shapes. Techniques based on binding forces can be used to develop (non-spherical branching growth) by attaching the smaller particle units together. Such techniques are outside the scope of the present work; however, they can be found in the works cited in the introduction (e.g. that of Blum & Wurm (2000)) and are currently being pursued by the author.

4. Work calculation and decomposition of impact events

Let us consider a decomposition of the impact event into a compression and recovery phase, i.e. $\delta\tau = \delta\tau_1 + \delta\tau_2$, between a pair of particles in a binary impact (figure 2). Between the compression and recovery phases, the particles achieve a common velocity, denoted v_{cn}. We may write for particle i

$$\left.\begin{aligned} \text{compression}: \quad & m_i v_{i\mathrm{n}}(0) + \int_0^{\delta\tau_1} I_{\mathrm{n}}(\tau)\,\mathrm{d}\tau = m_i v_{\mathrm{cn}}, \\ \text{recovery}: \quad & m_i v_{\mathrm{cn}} + \int_{\delta\tau_1}^{\delta\tau} I_{\mathrm{n}}(\tau)\,\mathrm{d}\tau = m_i v_{i\mathrm{n}}(\delta\tau), \end{aligned}\right\} \tag{4.1}$$

and for the other particle j

$$\left.\begin{aligned} &\text{compression}: && m_j v_{j\mathrm{n}}(0) - \int_0^{\delta\tau_1} I_{\mathrm{n}}(\tau)\,\mathrm{d}\tau = m_j v_{\mathrm{cn}}, \\ &\text{recovery}: && m_j v_{\mathrm{cn}} - \int_{\delta\tau_1}^{\delta\tau} I_{\mathrm{n}}(\tau)\,\mathrm{d}\tau = m_j v_{j\mathrm{n}}(\delta\tau), \end{aligned}\right\} \tag{4.2}$$

where v_{cn} is the common normal velocity achieved by both particles in a binary impact at the intermediate time of $\delta\tau_1$. This leads to

$$e \overset{\text{def}}{=} \frac{\int_{\delta\tau_1}^{\delta\tau} I_{\mathrm{n}}(\tau)\,\mathrm{d}\tau}{\int_0^{\delta\tau_1} I_{\mathrm{n}}(\tau)\,\mathrm{d}\tau} = \frac{v_{i\mathrm{n}}(\delta\tau) - v_{\mathrm{cn}}}{v_{\mathrm{cn}} - v_{i\mathrm{n}}(0)} = \frac{v_{\mathrm{cn}} - v_{j\mathrm{n}}(\delta\tau)}{v_{j\mathrm{n}}(0) - v_{\mathrm{cn}}}. \tag{4.3}$$

Clearly, if we eliminate v_{cn}, we recover the expression for e used earlier (equation (2.3)).

We consider a linear compression and recovery curve of the following form:

$$\left.\begin{aligned} &\text{compression}: && |I_{\mathrm{n}}(\tau)| = \frac{|I_{\mathrm{n}}^*|}{\delta\tau_1}(\tau), \\ &\text{recovery}: && |I_{\mathrm{n}}(\tau)| = |I_{\mathrm{n}}^*| - \frac{|I_{\mathrm{n}}^*|}{\delta\tau_2}(\tau - \delta\tau_1), \end{aligned}\right\} \tag{4.4}$$

which implies that $\bar{I}_{\mathrm{n}} = \frac{1}{2} I_{\mathrm{n}}^*$. The velocities are given by

$$\left.\begin{aligned} &\text{compression}: && v_{i\mathrm{n}}(\tau) = \frac{v_{\mathrm{cn}} - v_{i\mathrm{n}}(0)}{\delta\tau_1}(\tau) + v_{i\mathrm{n}}(0), \\ &\text{recovery}: && v_{i\mathrm{n}}(\tau) = \frac{v_{i\mathrm{n}}(\delta\tau) - v_{\mathrm{cn}}}{\delta\tau_2}(\tau - \delta\tau_1) + v_{\mathrm{cn}}, \\ &\text{compression}: && v_{j\mathrm{n}}(\tau) = \frac{v_{\mathrm{cn}} - v_{j\mathrm{n}}(0)}{\delta\tau_1}(\tau) + v_{j\mathrm{n}}(0), \\ &\text{recovery}: && v_{j\mathrm{n}}(\tau) = \frac{v_{j\mathrm{n}}(\delta\tau) - v_{\mathrm{cn}}}{\delta\tau_2}(\tau - \delta\tau_1) + v_{\mathrm{cn}}. \end{aligned}\right\} \tag{4.5}$$

These relations yield relative velocity expressions for the interface between the particles:

$$\left.\begin{aligned} &\text{compression}: && v_{i\mathrm{n}-j\mathrm{n}}(\tau) = v_{i\mathrm{n}}(\tau) - v_{j\mathrm{n}}(\tau) \\ &&& \quad = \underbrace{\frac{v_{j\mathrm{n}}(0) - v_{i\mathrm{n}}(0)}{\delta\tau_1}}_{\overset{\text{def}}{=} k_1}(\tau) + \underbrace{v_{i\mathrm{n}}(0) - v_{j\mathrm{n}}(0)}_{\overset{\text{def}}{=} k_2}, \\ &\text{recovery}: && v_{i\mathrm{n}-j\mathrm{n}}(\tau) = v_{i\mathrm{n}}(\tau) - v_{j\mathrm{n}}(\tau) \\ &&& \quad = \underbrace{\frac{v_{i\mathrm{n}}(\delta\tau) - v_{j\mathrm{n}}(\delta\tau)}{\delta\tau_2}}_{\overset{\text{def}}{=} k_3}(\tau - \delta\tau_1). \end{aligned}\right\} \tag{4.6}$$

The work done during the entire deformation history is given, for particle i, by

$$0 \leqslant \delta\mathcal{W} \stackrel{\text{def}}{=} |\mathcal{W}|_0^{\delta\tau_1} + \mathcal{W}|_{\delta\tau_1}^{\delta\tau}| = \left| \int_0^{\delta\tau_1} |I_{\text{n}}(\tau)| v_{i\text{n}-j\text{n}}(\tau)\,\mathrm{d}\tau + \int_{\delta\tau_1}^{\delta\tau} |I_{\text{n}}(\tau)| v_{i\text{n}-j\text{n}}(\tau)\,\mathrm{d}\tau \right|, \tag{4.7}$$

where, after integration,

$$\mathcal{W}|_0^{\delta\tau_1} = \frac{|I^*|}{\delta\tau_1}\left(\frac{k_1\delta\tau_1^3}{3} + \frac{k_2\delta\tau_1^2}{2}\right) \tag{4.8}$$

and

$$\mathcal{W}|_{\delta\tau_1}^{\delta\tau} = |I^*|k_3\left(\frac{\delta\tau^2 - \delta\tau_1^2}{2} - \delta\tau_1\delta\tau_2 - \frac{1}{\delta\tau_2}\left(\frac{\delta\tau^3 - \delta\tau_1^3}{3} - (\delta\tau^2 - \delta\tau_1^2)\delta\tau_1 + \delta\tau_1^2\delta\tau_2\right)\right). \tag{4.9}$$

The first time-interval is given by

$$\int_0^{\delta\tau_1} (k_1(\tau) + k_2)\,\mathrm{d}\tau = b^* \quad \Rightarrow \quad \delta\tau_1 = \frac{b^*}{(v_{i\text{n}}(0) - v_{j\text{n}}(0))/2}, \tag{4.10}$$

where b^* is a length-scale for deformation that is proportional to the radius of the smaller of the two impacting particles, $b^* \propto \min(b_i, b_j)$. We define $b^* \stackrel{\text{def}}{=} \beta\min(b_i, b_j)$. The second time-scale is taken to be $\delta\tau_2 = e\delta\tau_1$. We note that this accounts for the possibility that the recovery time is zero when the impact results in complete adhesion (perfectly plastic, $e = 0$). Also, the total work done is zero if the impact is perfectly elastic.

Remark 4.1. One can directly obtain an estimate on the relative normal velocities needed for particle agglomeration by setting $e = 0$ in equations (2.4), (2.5) and (3.1). Assuming $m_i = m_j = m$ yields

$$v_{i\text{n}-j\text{n}}^{\text{crit}} \stackrel{\text{def}}{=} v_{j\text{n}}(0) - v_{i\text{n}}(0) = \frac{4a^{\text{c}}H\delta\tau}{m}.$$

Since the particles are assumed to be spherical, the mass for each particle can be written as $m = \rho\frac{4}{3}\pi b^3$, where b is the radius. If we assume that the contact area is proportional to the cross-sectional area of the particles, $a^{\text{c}} = k\pi b^2$, $0 \leqslant k \leqslant 1$, then

$$v_{i\text{n}-j\text{n}}^{\text{crit}} = 3\frac{Hk\delta\tau}{b}. \tag{4.11}$$

In such a simple model, as b becomes larger, the critical velocity needed for adhesion becomes smaller, *provided that quantities like impact duration time and the contact area scaling are independent of particle size. However, this is unrealistic.* To correct this defect, we assume that the contact area scales with the severity of impact, characterized by e. A relatively simple way to express this is by a linear function of the coefficient of restitution and cross-sectional area of the smaller of the two contacting bodies (figure 2):

$$a^{\text{c}} = (a_0 + (a_{\text{f}} - a_0)(1 - e))\pi(\min(b_i, b_j))^2. \tag{4.12}$$

As an example of how this relation can be used, consider two identical particles approaching one another with velocity $v_p(0)$. Thus, we have

$$e \stackrel{\text{def}}{=} \frac{v_p(\delta\tau)}{v_p(0)} \approx \max\left(1 - \frac{|\bar{I}_{\text{n}}|/a^{\text{c}}}{2H}, 0\right) = \max\left(1 - \frac{m_i|v_p(\delta\tau) - v_p(0)|}{2a^{\text{c}}H\delta\tau}, 0\right). \quad (4.13)$$

Let us assume that $e \geqslant 0$ (an assumption that we shall check momentarily). After some lengthy algebra we have

$$e^2 + c_1 e + c_2 = 0 \quad \Rightarrow \quad e = \tfrac{1}{2}\Big(- c_1 \pm \sqrt{c_1^2 - 4c_2}\Big), \quad (4.14)$$

where the non-dimensional terms are

$$c_1 = \frac{\lambda - (a_0 - 2a_{\text{f}})}{a_0 - a_{\text{f}}}, \quad c_2 = \frac{\lambda - a_{\text{f}}}{a_0 - a_{\text{f}}} \quad \text{and} \quad \lambda = \frac{2\rho v_p^2(0)}{3H\beta}.$$

Now we make the logical choices $\beta = 1$, $a_{\text{f}} = 1$ and $a_0 = 0$. *There are no adjustable parameters.* The critical velocity for adhesion can be obtained from equation (4.14) by setting $e = 0$:

$$v_p(0) = \sqrt{\frac{3a_{\text{f}}H\beta}{2\rho}}. \quad (4.15)$$

Remark 4.2. Self-gravity becomes important in another phase of the agglomeration regime for larger 'particles' (relative to the problem at hand) approximately when (for example, between two such particles)

$$\frac{G(\frac{4}{3}\rho\pi b^3)^2}{(2b)^2} \approx 2Hb^2\pi \quad \Rightarrow \quad b = \frac{3}{\rho}\left(\frac{H}{2\pi G}\right)^{1/2}, \quad (4.16)$$

where $G = 6.673 \times 10^{-11}\ \text{m}^3\,\text{kg}^{-1}\,\text{s}^{-2}$ is the universal gas constant. For material parameter ranges considered in the present work, particles of the order of several kilometres in diameter are needed for self-gravity to affect the agglomeration. However, in many cases, near-field interaction due to surface charges—which, in a mathematical sense, is formally similar to gravity—can play a dominant role in the system dynamics for fine-scale grains. However, incorporation of these effects is beyond the scope of this work.

Remark 4.3. During the calculations, at time t, the tangential velocities, which are orthogonal to the normal direction, are computed by the difference of $\boldsymbol{v}_{\tan}(0) = \boldsymbol{v}(0) - \boldsymbol{v}_{\text{n}}(0)$, where $\boldsymbol{v}_{\text{n}}(0)$ is the $(\boldsymbol{v}(0)\cdot\boldsymbol{n})\cdot\boldsymbol{n}$. The normal direction, for two particles of different size contacting one another, is determined by the difference in the position vectors of their centres,

$$\boldsymbol{n}^{ji} = \frac{\boldsymbol{r}_j - \boldsymbol{r}_i}{\|\boldsymbol{r}_j - \boldsymbol{r}_i\|}.$$

Immediately after impact the tangential velocities are computed by a conservation of momentum in the tangential plane. For the impacting pair as a whole, we have, in the tangential plane, $m_i\boldsymbol{v}_{\tan,i}(0) + m_j\boldsymbol{v}_{\tan,j}(0) = m_i\boldsymbol{v}_{\tan,i}(\delta\tau) + m_j\boldsymbol{v}_{\tan,j}(\delta\tau)$. If there is permanent adhesion, dictated by $P \geqslant 2H$, then $\boldsymbol{v}_{\tan,i}(\delta\tau) = \boldsymbol{v}_{\tan,j}(\delta\tau)$. If the particles do not permanently adhere, then a balance of momentum for each particle

in the tangential direction dictates—under the assumption of Coulomb-type friction, $\mu|\bar{I}_{\mathrm{n}}|$ = friction force opposite to the direction of relative motion—that

$$\left.\begin{aligned}\boldsymbol{v}_{\mathrm{tan},i}(\delta\tau) &= -\frac{\mu|\bar{I}_{\mathrm{n}}|\delta\tau}{m_i}\frac{\boldsymbol{v}_{\mathrm{tan},i}(0)-\boldsymbol{v}_{\mathrm{tan},j}(0)}{\|\boldsymbol{v}_{\mathrm{tan},i}(0)-\boldsymbol{v}_{\mathrm{tan},j}(0)\|}+\boldsymbol{v}_{\mathrm{tan},i}(0),\\ \boldsymbol{v}_{\mathrm{tan},j}(\delta\tau) &= \frac{\mu|\bar{I}_{\mathrm{n}}|\delta\tau}{m_j}\frac{\boldsymbol{v}_{\mathrm{tan},i}(0)-\boldsymbol{v}_{\mathrm{tan},j}(0)}{\|\boldsymbol{v}_{\mathrm{tan},i}(0)-\boldsymbol{v}_{\mathrm{tan},j}(0)\|}+\boldsymbol{v}_{\mathrm{tan},j}(0).\end{aligned}\right\} \tag{4.17}$$

We again remark that the grains are idealized as small particles, and as such their rotation with respect to their centres of mass is deemed to be insignificant. Consequently, any energy lost due to rotation about their centres of mass is also deemed insignificant. Clearly, as the agglomerations grow, such an assumption is increasingly in error.

5. A simple fragmentation model

Clearly, during the impact process, there is a possibility that the particles formed from agglomerated particles may (re-)fragment during impact. The simple ad hoc criterion that we employ is based upon the (critical) amount of kinetic energy absorbed during impact. We proceed by equating the amount of kinetic energy absorbed with the amount of surface energy of fragments that would result from an entire agglomerated particle. This is characterized by

$$\delta\mathcal{K} = |\tfrac{1}{2}m\boldsymbol{v}(\delta\tau)\cdot\boldsymbol{v}(\delta\tau) - \tfrac{1}{2}m\boldsymbol{v}(0)\cdot\boldsymbol{v}(0)| = \gamma(n4\pi b^2 - 4\pi b_0^2) \stackrel{\mathrm{def}}{=} \delta\mathcal{Z}, \tag{5.1}$$

where n is the number of fragmented pieces (assumed to be spherical) each of radius b contained in the original particle, b_0 is the radius of the entire, unfragmented, particle before impact, $\delta\mathcal{Z}$ is the amount of energy released, and γ is the amount of energy per unit surface area. Since $n = b_0^3/b^3$, one obtains

$$b = b_0\left(\frac{1}{(\delta\mathcal{K}b_0/3\gamma V_0)+1}\right). \tag{5.2}$$

The criterion for fragmentation is

$$\left.\begin{aligned}&\text{if } b > b_0\text{, no fragmentation occurs} && (\delta\mathcal{Z}=0),\\ &\text{if } b \leqslant b_0\text{, fragment into } n = b_0^3/b^3 \text{ particles} && (\delta\mathcal{Z}\neq 0).\end{aligned}\right\} \tag{5.3}$$

Remark 5.1. Consider again the case describing particle–particle impact. Now consider fragmentation under the same conditions, but in the limiting case of $b = \frac{1}{2}b_0$ ($n = 2$), which leads to

$$v_p(0) = \sqrt{\frac{6\gamma}{\rho(1-e^2)b_0}}. \tag{5.4}$$

Now consider the special case of $e = 0$. Equating equations (4.15) and (5.4) leads to an expression for the critical size of the particle which would either stick (grow) or fragment:

$$b_0 = \frac{4\gamma}{Ha_{\mathrm{f}}\beta}. \tag{5.5}$$

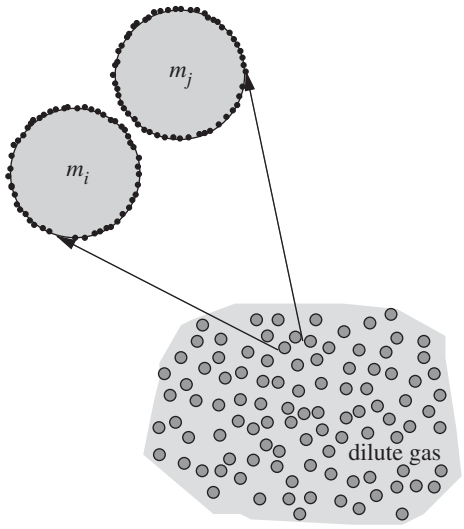

Figure 3. Presence of a dilute reactive gas adsorbed onto the surface of two impacting particles.

This expression implies that

(i) larger surface energy needed for fracture, γ, leads to larger particles,

(ii) smaller hardness, H, leads to larger particles,

(iii) smaller compression length-scales needed for adhesion, β, leads to larger particles, and

(iv) smaller critical contact area needed for adhesion, a_f, leads to larger particles.

Remark 5.2. The fragmentation criterion used is a massive simplification of an extremely complex event. For example, it is assumed that refragmentation occurs by the agglomerate being converted into N equal-sized particles. This is clearly an extreme oversimplification. In reality, oblique impact will probably cause 'chipping' to occur, leading to a number of large irregular-shaped agglomerates. Such an analysis is outside the scope of the present analysis. However, we refer the reader to Meyers (1994) for more details.

6. Thermochemical effects

The reactivity of particles in a granular flow can strongly affect the mechanics of impact, for example, due to thermal softening. For instance, the presence of a reactive substance (gas) adsorbed onto the surface of interplanetary dust can be a source of intense heat generation (figure 3). Due to reactive materials present on the particle surfaces, a rapidly formed molten layer may be generated which, upon cooling, strongly fuses the colliding pair together. Such effects thermally soften the material, which greatly enhances bonding. This effect has been exploited in the materials-processing community by purposely adding powdered hydrides and other potentially reactive materials into powder mixes of normally inert materials, such as silicon, to

enhance thermochemical bonding upon compaction. Generally, such reactions read as follows (Meyers 1994):

$$\underbrace{a_x b}_{\text{inert particles}} + \underbrace{(c+d)}_{\text{reactive mixture}} \rightarrow \underbrace{a_x b + c_y d}_{\text{fused solid}}. \tag{6.1}$$

One such method is shock induced chemical reactions (SICRs), whereby a shock wave is passed through reacting powders and sinters them together. Relevant work in the modelling and simulation of such processes may be found in Thadhani (1993), Nesterenko *et al.* (1994), Vecchio & Meyers (1994), Meyers *et al.* (1994), Meyers (1994) and recently in Do & Benson (2001). For example, the presence of hydrogen (H_2), silicon hydride (SiH_4) and oxygen (O_2) gases alone will produce silicon oxide (SiO_2) via†

$$SiH_4(\text{gas}) + 2O_2(\text{gas}) \longrightarrow SiO_2(\text{solid}) + 2H_2O(\text{gas}). \tag{6.2}$$

Quantities such as the mechanical hardness of a material, H, are thermally dependent. One possible representation of the hardness is by $H = H_0 \mathrm{e}^{Q/R\theta}$, where H_0 is the hardness at absolute zero, θ is the particle temperature, Q is an activation energy, and R is the universal gas constant. This is motivated by the fact that defect movement such as dislocation dynamics are frequently governed by such an Arrhenius-type relation. Thus, parameters such as the coefficient of restitution, which depend strongly on the hardness, implicitly depend on the temperature. In order to include thermal effects, we shall decompose the heat-transfer processes that particles in a granular flow experience into two stages. Stage I describes the extremely short time-interval when impact occurs, $\delta t \ll \Delta t$, and accounts for the effects of chemical reactions, which are relevant in certain applications, and energy release due to mechanical straining. Stage II accounts for the post-impact behaviour involving convective and radiative effects.

(*a*) *Stage I: an energy balance during impact*

Throughout the analysis, we shall use the most simplified models possible. Consistent with the particle-based philosophy, it is assumed that the temperature fields are uniform in the particles.‡ We consider an energy balance, governing the interconversions of mechanical, thermal and chemical energy in a system, dictated by the first law of thermodynamics. Accordingly, we require the time rate of change of the sum of the kinetic energy ($\mathcal{K}$) and stored thermal energy ($\mathcal{S}$) to be equal to the work rate (power, $\mathcal{P}$), the net heat supplied ($\mathcal{H}$) and the time rate of energy liberated during fracture ($\mathcal{Z}$), i.e.

$$\frac{\mathrm{d}}{\mathrm{d}t}(\mathcal{K} + \mathcal{S}) = \mathcal{P} + \mathcal{H} - \mathcal{Z}, \tag{6.3}$$

which upon integrating through the impact time-interval yields

$$\mathrm{d}\mathcal{K} + \mathrm{d}\mathcal{S} = \int_t^{t+\delta t} \mathcal{P}\,\mathrm{d}t + \int_t^{t+\delta t} \mathcal{H}\,\mathrm{d}t - \int_t^{t+\delta t} \mathcal{Z}\,\mathrm{d}t. \tag{6.4}$$

† A detailed breakdown of the materials possible in a gaseous protoplanetary accretion disc can be found in, among others, Pollack *et al.* (1994).

‡ Thus, the gradient of the temperature within the particle is zero, i.e. $\nabla\theta = \mathbf{0}$. Thus, a Fourier-type law for the heat flux will register a zero value.

Thus, for an arbitrary particle in the flow,

$$\mathcal{S}(t+\delta t) = \mathcal{S}(t) + \mathcal{K}(t) - \mathcal{K}(t+\delta t) + \int_t^{t+\delta t} (\mathcal{P} + \mathcal{H} - \mathcal{Z})\,\mathrm{d}t, \tag{6.5}$$

where the stored thermal energy is $\mathcal{S}(t) = mC\theta(t)$, where C is the heat capacity per unit mass, and the kinetic energy is $\mathcal{K}(t) = \frac{1}{2}m\boldsymbol{v}(t)\cdot\boldsymbol{v}(t)$. The integral of the mechanical power term is

$$\int_t^{t+\delta t} \mathcal{P}\,\mathrm{d}t = \delta\mathcal{W}. \tag{6.6}$$

The energy liberated from fracture is (as governed by equations (5.1) and (5.3))

$$\int_t^{t+\delta t} \mathcal{Z}\,\mathrm{d}t = \delta\mathcal{Z}. \tag{6.7}$$

The primary source of heat is due to chemical reactions. Here it is assumed that the chemical species acts as a catalyst which promotes reactions. The chemical reaction energy is defined as

$$\delta\mathcal{H} \stackrel{\text{def}}{=} \int_t^{t+\delta t} \mathcal{H}\,\mathrm{d}t$$

and will be discussed in more detail shortly. Equation (6.5) can be rewritten for the temperature at time$=t+\delta t$ as

$$\theta(t+\delta t) = \theta(t) + \frac{1}{mC}(\delta\mathcal{K} + \delta\mathcal{W} + \delta\mathcal{H} - \delta\mathcal{Z}), \tag{6.8}$$

where $\delta\mathcal{K} \stackrel{\text{def}}{=} \mathcal{K}(t) - \mathcal{K}(t+\delta t)$. The energy released from the reactions are assumed to be proportional to the amount of the gaseous substance available to be compressed in the contact area between the particles. A typical, ad hoc approximation in combustion processes is to write

$$\delta\mathcal{H} = \alpha a^{\mathrm{c}}, \tag{6.9}$$

where α is a reaction constant (for details see, for example, Schmidt (1998)). Thus, we have

$$\theta(t+\delta t) = \theta(t) + \frac{1}{2C}(\boldsymbol{v}(t)\cdot\boldsymbol{v}(t) - \boldsymbol{v}(t+\delta t)\cdot\boldsymbol{v}(t+\delta t)) + \frac{1}{mC}(\delta\mathcal{W} + \delta\mathcal{H} - \delta\mathcal{Z}). \tag{6.10}$$

The temperature rise affects the hardnesses of the impacting materials. As indicated earlier, two surfaces will bond when pressed together if the magnitude of the surface pressure (P) exceeds or attains twice the Vicker's hardness ($2H$), i.e. if $|P| \geqslant 2H$. Thus, heated particles will bond more easily due to thermal softening. *Clearly, these equations are coupled to those of impact through the coefficient of restitution.* Additionally, since the post-collision velocities are computed from the momentum relations, the terms on the right-hand side of equation (6.10) are coupled to the temperature. Later in the analysis, this equation is incorporated into an overall staggered fixed-point iteration scheme, whereby the temperature is predicted for a given velocity field, and then the velocities are recomputed with the new temperature field, etc. The process is repeated until the fields change negligibly between successive iterations. The entire set of equations are embedded within a larger overall set of equations later in the analysis, and solved in a recursively staggered manner.

Remark 6.1. One notices that water is produced in gaseous form by the reactions in equation (6.2), thus leading to possible frost layers around the particulates. The role of frost in the bonding and formation of bodies has been noted in numerous articles (for example in Supulver & Lin (2000)).

Remark 6.2. Most processed powdered materials are normally difficult to bond together without thermochemical treatment, even when extremely high pressures are applied (for reviews, see Anand & Gu (2000), Gu *et al.* (2001), Akisanya *et al.* (1997), Fleck (1995), Brown & Abou-Chedid (1994), Zohdi *et al.* (2002*a*) and Zohdi (2003*b*)). Generally speaking, the analysis of the compaction of metallic powders is closely related to the pioneering work of Gurson (1977) addressing void growth and coalescence at finite elasto-plastic strains. For background information on the development of this widely used model we refer the reader to Pardoen & Hutchinson (2000).

(*b*) *Multi-field staggering schemes*

To solve the coupled problem we employ a staggering scheme, whereby, within a time-step, each field equation is solved individually, allowing only the primary field variable to be active. After the solution of each field equation, the primary field variable is updated, and the next field equation is addressed in a similar manner. Such approaches have a long history in the computational mechanics community (see, for example, Park & Felippa 1983; Zienkiewicz 1984; Schrefler 1985; Lewis *et al.* 1992; Doltsinis 1993, 1997; Piperno 1997; Lewis & Schrefler 1998; Le Tallec & Mouro 2001). Here we extend the methodology found in Zohdi (2002*b*) to the class of problems at hand. We consider an abstract setting, where one can consider the following abstract active set solution strategy:

$$\left.\begin{aligned} \mathcal{A}_1(\underline{\boldsymbol{v}^{L+1,K+1}}, \theta^{L+1,K}) &= \mathcal{F}_1(\boldsymbol{v}^{L+1,K}, \theta^{L+1,K}) \qquad \text{(particle velocities)},\\ \mathcal{A}_2(\boldsymbol{v}^{L+1,K+1}, \underline{\theta^{L+1,K+1}}) &= \mathcal{F}_2(\boldsymbol{v}^{L+1,K+1}, \theta^{L+1,K}) \qquad \text{(thermal fields)}, \end{aligned}\right\} \tag{6.11}$$

where only the underlined variable is 'active', where L indicates the time-step, and where K indicates the iteration counter. This approach can be interpreted as a fixed-point iteration within a time-step where the overall system is written as $\mathcal{A}(\boldsymbol{w}) = \mathcal{F}$, where $\boldsymbol{w} = (\boldsymbol{v}, \theta)$. Performing an operator split yields

$$\mathcal{A}(\boldsymbol{w}) - \mathcal{F} = \mathcal{G}(\boldsymbol{w}) - \boldsymbol{w} + \mathcal{E} = \boldsymbol{0}, \tag{6.12}$$

where $\mathcal{E} \neq \mathcal{E}(\boldsymbol{w})$ is a (remainder) term that does not depend on the solution. This can be used to develop an iterative scheme

$$\boldsymbol{w}^K = \mathcal{G}(\boldsymbol{w}^{K-1}) + \mathcal{E}. \tag{6.13}$$

As is well known, the convergence of such a scheme is dependent on the eigenvalues of $\mathcal{G}$, namely, with relatively mild assumptions, if the magnitude of the eigenvalues are less than one, convergence to a solution is assured (see Axelsson (1994) for general remarks and Zohdi (2002*b*, 2003*a*, *d*) for specifics pertaining to particulate systems). In this approach, the system is repeatedly re-solved until fixed-point-type convergence is achieved. Also, in order for the simulations to accurately capture the impact scenarios one must scale the time-step discretization sizes in such a way as to

not overshoot the gaps between the moving particles. Proceeding along these lines, during the simulations to be described in more detail momentarily, the time-steps are determined by ascertaining the minimum-gap distance divided by the relative velocity between nearest neighbours. This is approximately determined by scanning over all of the ith particle's nearest neighbours after each time-step during the simulations ($\|\boldsymbol{v}_{i\mathrm{n}} - \boldsymbol{v}_{j\mathrm{n}}\| \neq 0$):

$$\Delta t \propto \min_{i,j}\left(\frac{\|\boldsymbol{r}_i - \boldsymbol{r}_j\|}{\|\boldsymbol{v}_{i\mathrm{n}} - \boldsymbol{v}_{j\mathrm{n}}\|}\right), \tag{6.14}$$

where i and j signify nearest-neighbour pairs. Furthermore, we remark that $\delta\tau \ll \Delta t$, so that $\delta\tau$ can be neglected during the time-stepping portion of the algorithm. Also, typically, for the system at hand, convergence is easily attained over a wide parameter range, since at low speeds the contraction constant is small, and the iterations converge quickly, while at high speeds, the particles agglomerate ($e = 0$), and only a few iterations are necessary. Such iterative schemes are highly advantageous since any previous solution, from a previous time-step or staggered iteration, can be used as the first guess in the solution procedure, thus providing a 'head start' in the solution process. The specifics of the implementation of the multilevel (embedded) recursive staggering scheme are as follows within a time-step $(L+1)$.

Staggering scheme.

(1) For each particle (i) find nearest neighbour (j):

$$r_{j=p}^{L+1,K} \overset{\text{def}}{=} \min_{r_{p\neq i}^{L+1,K}} \|\boldsymbol{r}_i^{L+1,K} - \boldsymbol{r}_p^{L+1,K}\|.$$

(1.1) If in contact, assume a starting value ($K = 0$, $e^{L+1,K} = 0$).

(1.2) Compute the following for the contact pair:

$$\begin{aligned}
v_{i\mathrm{n}}^{L+1,K} &= \frac{m_i v_{i\mathrm{n}}^{L} + m_j(v_{j\mathrm{n}}^{L} - e^{L+1,K}(v_{i\mathrm{n}}^{L} - v_{j\mathrm{n}}^{L}))}{m_i + m_j},\\
v_{j\mathrm{n}}^{L+1,K} &= v_{i\mathrm{n}}^{L+1,K} + e^{L+1,K}(v_{i\mathrm{n}}^{L} - v_{j\mathrm{n}}^{L}),\\
\bar{I}_{\mathrm{n}}^{L+1,K} &= \frac{m_i(v_{i\mathrm{n}}^{L+1,K} - v_{i\mathrm{n}}^{L})}{(\delta\tau)^{L+1,K}},\\
\boldsymbol{v}_{\mathrm{tan},i}^{L+1,K} &= -\mu|\bar{I}_{\mathrm{n}}^{L+1,K}|(\delta\tau)^{L+1,K}\frac{\boldsymbol{v}_{\mathrm{tan},i}^{L} - \boldsymbol{v}_{\mathrm{tan},j}^{L}}{\|\boldsymbol{v}_{\mathrm{tan},i}^{L} - \boldsymbol{v}_{\mathrm{tan},j}^{L}\|} + \boldsymbol{v}_{\mathrm{tan},i}^{L},\\
\boldsymbol{v}_{\mathrm{tan},j}^{L+1,K} &= \mu|\bar{I}_{\mathrm{n}}^{L+1,K}|(\delta\tau)^{L+1,K}\frac{\boldsymbol{v}_{\mathrm{tan},i}^{L} - \boldsymbol{v}_{\mathrm{tan},j}^{L}}{\|\boldsymbol{v}_{\mathrm{tan},i}^{L} - \boldsymbol{v}_{\mathrm{tan},j}^{L}\|} + \boldsymbol{v}_{\mathrm{tan},j}^{L},\\
e^{L+1,K+1} &\overset{\text{def}}{=} \max\left(1 - \frac{m_i|v_{i\mathrm{n}}^{L+1,K} - v_{i\mathrm{n}}^{L}|}{2\min(H_i^{L+1,K}, H_j^{L+1,K})a^{c,L+1,K}(\delta\tau)^{L+1,K}}, 0\right).
\end{aligned}$$

If $|e^{L+1,K+1} - e^{L+1,K}| > (e^{L+1,K}) \times \mathrm{TOL}$, then $e^{L+1,K} = e^{L+1,K+1}$.

Update all quantities needed for

$$\theta_i^{L+1,K+1} = \theta_i^L + \frac{1}{m_i C}(\delta\mathcal{K} + \delta\mathcal{W} + \delta\mathcal{H} - \delta\mathcal{Z})_i^{L+1,K+1},$$
$$\theta_j^{L+1,K+1} = \theta_j^L + \frac{1}{m_j C}(\delta\mathcal{K} + \delta\mathcal{W} + \delta\mathcal{H} - \delta\mathcal{Z})_j^{L+1,K+1},$$
$$H_i^{L+1,K+1} = H_0 \exp\left(\frac{Q}{R\theta_i^{L+1,K+1}}\right),$$
$$H_j^{L+1,K+1} = H_0 \exp\left(\frac{Q}{R\theta_j^{L+1,K+1}}\right).$$

Go to (1.2) and repeat with new system values.
If $|e^{L+1,K+1} - e^{L+1,K}| \leqslant (e^{L+1,K}) \times \mathrm{TOL}$, then go to (1.1) for next contact pair.

(2) If all contact pairs are finished, update agglomeration and system variable states.

Go to (1) with adapted time-step size:

$$\Delta t = \min_{i,j}\left(\frac{\|\boldsymbol{r}_i^{L+1,K+1} - \boldsymbol{r}_j^{L+1,K+1}\|}{\|\boldsymbol{v}_{i\mathrm{n}}^{L+1,K+1} - \boldsymbol{v}_{j\mathrm{n}}^{L+1,K+1}\|}\right).$$

Remark 6.3. An alternative approach might be the use of a gradient-based scheme, such as Newton's method, since they usually converge at a faster rate than a direct fixed-point iteration, quadratic as opposed to superlinear. For example, consider the residual

$$\mathcal{R} \stackrel{\mathrm{def}}{=} \mathcal{A}(\boldsymbol{w}) - \mathcal{F}.$$

Linearization leads to

$$\mathcal{R}(\boldsymbol{w}^K) = \mathcal{R}(\boldsymbol{w}^{K-1}) + (\nabla_{\boldsymbol{w}}\mathcal{R}(\boldsymbol{w}))|_{\boldsymbol{w}^{K-1}}(\boldsymbol{w}^K - \boldsymbol{w}^{K-1}) + \mathcal{O}(\|\Delta\boldsymbol{w}\|^2), \tag{6.15}$$

and thus the Newton updating scheme can be developed by enforcing $\mathcal{R}(\boldsymbol{w}^K) \approx \boldsymbol{0}$, leading to

$$\boldsymbol{w}^K = \boldsymbol{w}^{K-1} - (\mathcal{A}^{\mathrm{TAN},K-1})^{-1}\mathcal{R}(\boldsymbol{w}^{K-1}), \tag{6.16}$$

where

$$\mathcal{A}^{\mathrm{TAN},K-1} = (\nabla_{\boldsymbol{w}}\mathcal{A}(\boldsymbol{w}))|_{\boldsymbol{w}^{K-1}} = (\nabla_{\boldsymbol{w}}\mathcal{R}(\boldsymbol{w}))|_{\boldsymbol{w}^{K-1}} \tag{6.17}$$

is the tangent. Therefore, in the fixed-point form one has the operator form

$$\mathcal{G}(\boldsymbol{w}) = \boldsymbol{w} - (\mathcal{A}^{\mathrm{TAN}})^{-1}\mathcal{R}(\boldsymbol{w}). \tag{6.18}$$

For the problems considered, it is unlikely that the gradients of $\mathcal{A}$ remain positive definite, or even that $\mathcal{A}$ is continuously differentiable, due to the impact events. Essentially, $\mathcal{A}$ will have non-convex and non-differentiable dependence on the velocities and temperatures of the particles. Thus, a fundamental difficulty is the possibility of a zero or non-existent tangent ($\mathcal{A}^{\mathrm{TAN}}$), thus making a standard gradient-based scheme's range of applicability less robust.

(c) *Stage II: post-collision thermal behaviour*

After impact, it is assumed that a process of convection, for example governed by Newton's law of cooling, and radiation according to a simple Stefan–Boltzmann law transpires. As before, it is assumed that the temperature fields are uniform within the particles, thus conduction within the particles is negligible.† *We also assume that the state of the gas is insensitive to the particles.* The first law reads

$$\frac{\mathrm{d}(K+U)}{\mathrm{d}t} = m\dot{\boldsymbol{v}}\cdot\boldsymbol{v} + mC\dot{\theta} = -\underbrace{h_{\mathrm{c}}a_{\mathrm{s}}(\theta-\theta_0)}_{\text{convective heating}} - \underbrace{\mathcal{B}a_{\mathrm{s}}\varepsilon(\theta^4-\theta_{\mathrm{s}}^4)}_{\text{far-field radiation}}, \tag{6.19}$$

where θ_0 is the temperature of the ambient gas, where θ_{s} is the temperature of the far field surface (for example, a container surrounding the flow) with which radiative exchange is made, $\mathcal{B} = 5.67\times10^{-8}\ \mathrm{W\,m^{-2}\,K^{-1}}$ is the Stefan–Boltzmann constant, where $0 \leqslant \varepsilon \leqslant 1$ is the emissivity, which indicates how efficiently the surface radiates energy compared with a black body (an ideal emitter), where $0 \leqslant h_{\mathrm{c}}$ is the heating due to convection (Newton's law of cooling) into the dilute gas. It is assumed that the radiation exchange between the particles is negligible. For the applications considered, typically, h_{c} is quite small, and plays a small role in the heat-transfer processes.‡ From a balance of momentum we have $m\dot{\boldsymbol{v}} = \boldsymbol{0}$ after impact, and equation (6.19) becomes

$$mC\dot{\theta} = -h_{\mathrm{c}}a_{\mathrm{s}}(\theta-\theta_0) - \mathcal{B}a_{\mathrm{s}}\varepsilon(\theta^4-\theta_{\mathrm{s}}^4). \tag{6.20}$$

Therefore, after a single forward Euler integration, with the previously used finite-difference time-step of $\Delta t \gg \delta t$, implying $\theta(t) = \theta(t+\delta t)$, where $\theta(t+\delta t)$ is computed, in an explicit manner, from equation (6.10) to yield

$$\theta(t+\Delta t) = \theta(t) - \frac{\Delta t}{mC}(h_{\mathrm{c}}a_{\mathrm{s}}(\theta(t)-\theta_0) + \mathcal{B}a_{\mathrm{s}}\varepsilon(\theta^4(t)-\theta_{\mathrm{s}}^4)). \tag{6.21}$$

Furthermore, to update each particle position (explicitly), we compute $\boldsymbol{r}(t+\Delta t) = \boldsymbol{r}(t) + \Delta t\boldsymbol{v}(t+\Delta t)$.

Remark 6.4. Convection heat transfer is comprised of two primary mechanisms, one due to primarily random molecular motion (diffusion) and the other by bulk motion of a fluid, in our case a gas, surrounding the particles. As we have indicated, in the applications of interest here, the gas is dilute and the Reynold's number is small, thus convection plays a very small role in the heat-transfer process.¶

Remark 6.5. We recall that a black body is an ideal radiating surface having the following properties.

(i) A black body absorbs all incident radiation, regardless of wavelength and direction.

† The Biot number for spheres scale with the ratio of volume to surface area, $V/a_{\mathrm{s}} = \frac{1}{3}b$, thus a lumped mass approximation is quite reasonable.

‡ The Reynolds number, which measures the ratio of the inertial forces to viscous forces in the surrounding gas, and dictates the magnitude of these parameters, is extremely small in the regimes considered.

¶ During the upcoming computational simulations, we chose an emissivity of $\varepsilon = 0.5$, $h_{\mathrm{c}} = 0$ and $\theta_{\mathrm{s}} = 300$ K.

(ii) For a prescribed temperature and wavelength, no surface can emit more energy than a black body.

(iii) Although the radiation emitted by a black body is a function of wavelength and temperature, it is independent of direction.

Since a black body is a perfect emitter, it serves as a standard against which the radiative properties of actual surfaces may be compared. The Stefan–Boltzmann law, which is computed by integrating the classical Planck representation of the emissive power distribution of a black body over all wavelengths, allows the calculation of the amount of radiation emitted in all directions and over all wavelengths simply from the knowledge of the temperature of the black body.

7. Maximization of agglomeration likelihood

We now concentrate on constructing inverse problems where transient flow conditions, reaction rates, particulate volume fractions, hardnesses, etc., are sought that maximize growth from a base starting particulate size. We constructed the following normalized cost function to minimize

$$\Pi = \left(1 - \frac{b^{\mathrm{f}}}{b^*}\right), \tag{7.1}$$

where b^{f} is the final average radius of the particles in a control volume and b^* is the radius of a hypothetical agglomerated particle containing all of the original particles in the system. By setting b^* to be the radius of a particle with the mass of all of the particles agglomerated together, we require the algorithm to maximize the agglomeration likelihood. The average number of particles in an agglomeration, denoted n, can be determined by

$$n^{\mathrm{f}} \stackrel{\mathrm{def}}{=} \left(\frac{b^{\mathrm{f}}}{b^0}\right)^3 = \left(\frac{(1-\Pi)b^*}{b^0}\right)^3, \tag{7.2}$$

where b^0 is the initial radius of the particles. Due to the fact that objective functions such as Π depend in a non-convex and non-differentiable manner on the mentioned starting-state parameters, gradient-based minimization methods are inapplicable. The lack of *robustness* of gradient-based deterministic minimization processes can be rectified by application of a family of methods, usually termed 'genetic' algorithms. Genetic algorithms are search methods based on the principles of natural selection, employing concepts of species evolution, such as reproduction, mutation and crossover. Such methods have followed from the pioneering work of Holland (1975). For reviews of such methods, the interested reader is referred to Goldberg (1989), Davis (1991) and Onwubiko (2000). A recent overview of the state of the art of the field can be found in a collection of articles edited by Goldberg & Deb (2000).

In Zohdi (2003*a*, *c*) a genetic algorithm was developed, where the key feature was the development of a 'genetic string', which contains parameter set information. A 'survival-of-the-fittest' algorithm was then applied to a population of such strings. The term 'fitness' of a genetic string indicates the value of the objective function. The most-fit genetic string is the one with the smallest objective function. In this

presentation, we concentrate on adapting this type of genetic algorithm to inverse problems. Accordingly, we write the state vector as a string

$$\boldsymbol{\Lambda} \stackrel{\text{def}}{=} (\boldsymbol{v}^0_{\text{rel}}, \mathcal{L}, \rho, H_0, C, \mu, \theta_0, Q, \alpha, \gamma), \tag{7.3}$$

where $\mathcal{L}$ indicates a length-scale of the particles, and where the other parameters have been introduced earlier. The particle size and volume fraction are determined by a particle/sample size ratio, which is defined via a subvolume size

$$V \stackrel{\text{def}}{=} (D \times D \times D)/n,$$

where n is the number of particles in the entire sample of dimensions $D \times D \times D$. The ratio between the radius (b) and the subvolume are related by

$$\mathcal{L} \stackrel{\text{def}}{=} b/V^{1/3}.$$

The volume fraction occupied by the particles is

$$v_{\text{f}} \stackrel{\text{def}}{=} \tfrac{4}{3}\pi\mathcal{L}^3.$$

Thus, the total volume occupied by the particles, denoted Δ, can be written as $\Delta = v_{\text{f}} n V$ and the total mass $M = \sum_{i=1}^{n} m_i = \rho\Delta$, while that of an individual particle, before agglomeration begins, assuming that all are the same size, is $m_i = \rho\Delta/n = \rho\frac{4}{3}\pi b_i^3$. We considered starting-state vectors, constrained within prespecified search ranges, consisting of the relative velocity vector distribution, perturbed around a mean value $\boldsymbol{v}_{\text{rel}} = \boldsymbol{v}^0_{\text{rel}}\lambda_i$, where $-1 \leqslant \lambda_i \leqslant 1$, for each ($i$) particle. During the simulation of groups of particles, if a particle escapes from the control volume, the position component is reversed and the same velocity component is retained (now incoming). For example, if the x component of the position vector exceeds the boundary of the control volume, then $r_{ix} = -r_{ix}$ is enforced. The entire set of search variables and search space was

$$\left.\begin{array}{c} 20 \leqslant v^0_{x\text{rel}}\ \text{m s}^{-1} \leqslant 2 \times 10^2, \\ 0.4 \leqslant \mathcal{L} \leqslant 0.8, \\ 10^3 \leqslant \rho\ \text{kg m}^{-3} \leqslant 10^4, \\ 10^5 \leqslant \text{Pa} \leqslant 10^6, \\ 2 \times 10^2 \leqslant C\ \text{J kg}^{-1}\ \text{K}^{-1} \leqslant 2 \times 10^3, \\ 10^{-3} \leqslant \mu \leqslant 10^{-2}, \\ 10^2 \leqslant \theta_0\ \text{K} \leqslant 10^3, \\ 10^2 \leqslant Q\ \text{J mole}^{-1} \leqslant 10^3, \\ 10^{13} \leqslant \alpha\ \text{J m}^{-2} \leqslant 10^{14}, \\ 10^{15} \leqslant \gamma\ \text{J m}^{-2} \leqslant 10^{16}, \end{array}\right\} \tag{7.4}$$

where $v^0_{y\text{rel}} = v^0_{z\text{rel}} = 10\ \text{m s}^{-1}$, i.e. a velocity field with only a non-zero *mean* x velocity component. The mean velocity of the particulates was set to $v_{x0} = 10\ \text{m s}^{-1}$, $v_{y0} = 10\ \text{m s}^{-1}$ and $v_{z0} = 100\ \text{m s}^{-1}$. The relative velocity distributions (velocity

deviations from the mean) in the y- and z-directions were related to the one in the x-direction by $v^0_{y\mathrm{rel}} = v^0_{z\mathrm{rel}} = 0.1 v^0_{x\mathrm{rel}}$.

The following genetic algorithm, recently developed in Zohdi (2003*a*, *c*), was applied.

Step 1. Randomly select a population of S starting genetic strings, $\boldsymbol{\Lambda}^i$ $(i = 1, \ldots, S)$:

$$\begin{aligned}\boldsymbol{\Lambda}^i &\stackrel{\mathrm{def}}{=} \{\Lambda^i_1, \Lambda^i_2, \Lambda^i_3, \Lambda^i_4, \Lambda^i_5, \Lambda^i_6, \Lambda^i_7, \ldots, \Lambda^i_N\} \\ &= \{(\boldsymbol{v}^0_{\mathrm{rel}})^i, \mathcal{L}^i, \rho^i, H^i_0, C^i, \mu^i, \theta^i_0, Q^i, \alpha^i, \gamma^i\}.\end{aligned}$$

Step 2. Compute the fitness of each string $\Pi(\boldsymbol{\Lambda}^i)$ $(i = 1, \ldots, S)$.

Step 3. Rank the genetic strings: $\boldsymbol{\Lambda}^i$ $(i = 1, \ldots, S)$.

Step 4. Mate the nearest pairs and produce two offspring $(i = 1, \ldots, S)$:

$$\boldsymbol{\lambda}^i \stackrel{\mathrm{def}}{=} \Phi^{(\mathrm{I})}\boldsymbol{\Lambda}^i + (1 - \Phi^{(\mathrm{I})})\boldsymbol{\Lambda}^{i+1}, \qquad \boldsymbol{\lambda}^{i+1} \stackrel{\mathrm{def}}{=} \Phi^{(\mathrm{II})}\boldsymbol{\Lambda}^i + (1 - \Phi^{(\mathrm{II})})\boldsymbol{\Lambda}^{i+1}.$$

Note. $\Phi^{(\mathrm{I})}$ and $\Phi^{(\mathrm{II})}$ are random numbers, such that $0 \leqslant \Phi^{(\mathrm{I})}, \Phi^{(\mathrm{II})} \leqslant 1$, which are different for each component of each string.

Step 5. Kill off the bottom $M < S$ strings and keep the top $K < N$ parents and the top K offspring (K offspring + K parents + $M = S$).

Step 6. Repeat steps 1–6 with the top gene pool (K offspring and K parents) plus M new, randomly generated strings.

Option. Rescale and restart the search around best design every few generations.

Option. Gradient-based methods can be useful for post-processing solutions found with the genetic algorithm if the objective function is sufficiently smooth in that region of the parameter space. In the current work, we did not employ this post-genetic operation.

The retention of the top parent genetic strings is critical, since if, as for the present class of problems, the objective functions are highly non-convex, it will be likely that some inferior offspring will replace superior parents. When the top-performing parents are retained, with increasing generations, there will be guaranteed improvement, i.e. the minimization of the cost function is guaranteed to be monotonically decreasing. Successive improvement is not assured if the top performers are not retained, even though their non-retention allows for larger numbers of newer genetic strings to be evaluated in populations which come afterwards. Additionally, parent retention is computationally less expensive, since these parameter sets do not have to be re-evaluated in the next generation. For sufficiently large populations, numerical studies conducted by the author (Zohdi 2003*c*) indicate that the benefits of parent retention outweigh any disadvantages of 'inbreeding', i.e. a stagnant population. Such population characteristics are termed 'inheritance properties' and we refer the reader to Davis (1991) or Kennedy & Eberhart (2001) for more details. In the presented algorithm, inbreeding is mitigated in step 6 since, with each new generation, new parameter sets, selected at random within the parameter set space, are added to the population.

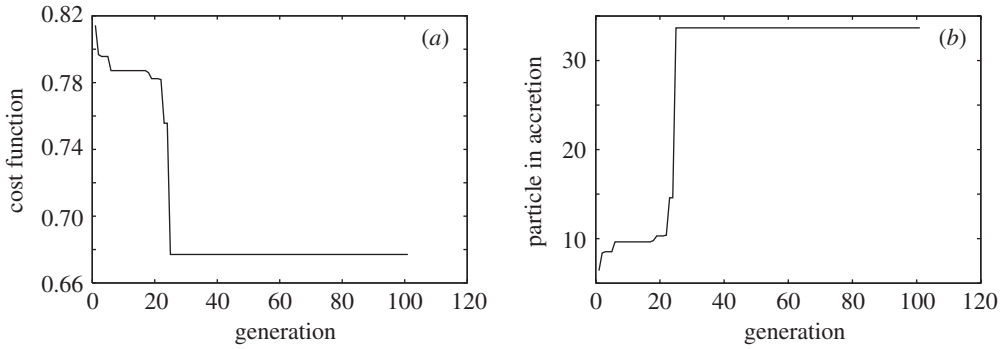

Figure 4. (*a*) The cost function for the best parameter set with each passing generation. (*b*) The corresponding average size of the agglomeration. After approximately 25 generations the search reached a steady-state value.

8. Numerical inverse simulations

We performed the inverse parameter identification for control volumes, each containing 1000 initially non-intersecting, equally sized particles. The objective was to maximize the diameter of the particles. This was parametrized as a minimization of the difference between the average diameter in the flow and the maximum possible diameter (b^*) containing all 1000 particles. Typically, for particle groups with a finite number of grains, a numerically generated (random) sample realization will not be perfectly statistically representative. Therefore, one must simulate several samples and then ensemble average the responses of the samples to obtain statistically valid objective functions. In order to stabilize the objective function's value with respect to the randomness of the sample starting configuration, for a fixed parameter set ($\boldsymbol{\Lambda}$), a regularization procedure is applied within the 'staggering scheme' on page 3434, whereby the performances of a series of different random starting configurations are averaged until the (ensemble) average converges, i.e. until the following condition is met ($i = 1, 2, \ldots, E$):

$$\left| \frac{1}{E+1} \sum_{i=1}^{E+1} \Pi^{(i)}(\boldsymbol{\Lambda}^I) - \frac{1}{E} \sum_{i=1}^{E} \Pi^{(i)}(\boldsymbol{\Lambda}^I) \right| \leqslant \mathrm{TOL} \left| \frac{1}{E+1} \sum_{i=1}^{E+1} \Pi^{(i)}(\boldsymbol{\Lambda}^I) \right|. \tag{8.1}$$

The index i indicates a starting random configuration that has been generated and E indicates the total number of configurations tested. In order to implement this into the genetic algorithm, in step 2, one replaces *compute* with *ensemble*, which requires a further inner loop to test the performance of multiple starting configurations. Similar ideas have been applied to randomly dispersed particulate solids in Zohdi (2003*a*, *c*).

A population of 20 genetic strings was selected per generation. The top six parents were retained after each generational 'mating sequence'. Six new offspring were produced from the top six parents, and allowed to proceed, along with their parents, to the next generation. Therefore, 14 old 'bad' genetic strings were eliminated and eight new genetic strings were infused after each generation. The initial position vectors were given random values, within each control volume of $-D \leqslant r_{ix}, r_{iy}, r_{iz} \leqslant D$. We selected $D = 0.01$ m. For each starting state a total simulation time was set to 0.01 s, using adaptive time-steps, adapted according to the criteria introduced earlier, limited to be between $10^{-8}\,\mathrm{s} \leqslant \Delta t \leqslant 10^{-3}\,\mathrm{s}$. After every four generations the search

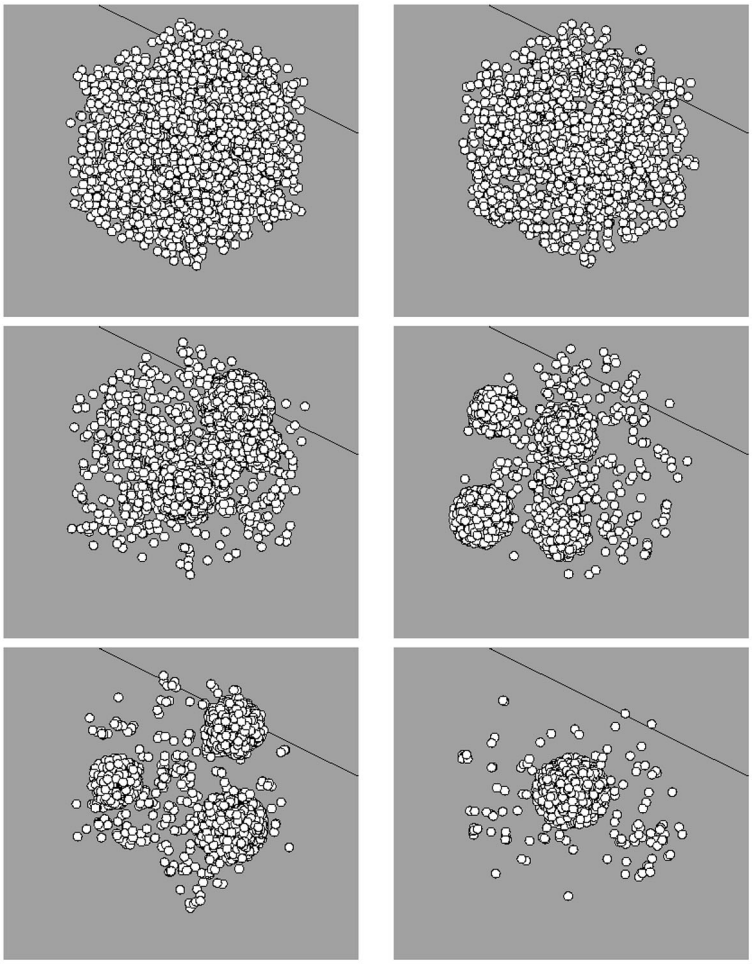

Figure 5. Starting from the top, left to right: an initially fine cloud of particles which agglomerates into a large particle. The *average mass* of the remaining particles was approximately 33.67 times greater than the mass of those initially, i.e. *on average*, 33.67 original-sized particles were in each remaining particle.

Table 1. *Best (normalized) starting-state vectors after 25 generations*

rank	$v^0_{x\mathrm{rel}}$ m s^{-1} $\times 0.5 \times 10^{-2}$	$\mathcal{L}$	ρ kg m^{-3} $\times 10^{-4}$	H_0 Pa $\times 10^{-6}$	C J kg^{-1} K^{-1} $\times 0.5 \times 10^{-3}$
1	0.923 44	0.790 41	0.665 27	0.265 48	0.898 15
2	0.993 07	0.795 10	0.905 09	0.490 48	0.940 75
3	0.960 42	0.797 26	0.667 73	0.397 72	0.342 35
4	0.939 11	0.792 80	0.532 28	0.204 59	0.989 42
5	0.849 77	0.792 26	0.917 91	0.156 71	0.969 95
6	0.167 61	0.793 62	0.939 62	0.108 77	0.956 69

Table 2. *Best (normalized) starting-state vectors after 25 generations*

rank	μ $\times 10^{-2}$	θ_0 K $\times 10^{-3}$	Q J mole^{-1} $\times 10^{-3}$	α J m^{-2} $\times 10^{-14}$	γ J m^{-2} $\times 10^{-16}$
1	0.134 56	0.502 18	0.352 41	0.177 65	0.836 85
2	0.175 35	0.624 94	0.124 57	0.208 36	0.852 67
3	0.110 00	0.219 11	0.197 85	0.199 01	0.934 62
4	0.156 24	0.903 23	0.385 58	0.152 09	0.913 21
5	0.104 55	0.362 70	0.323 26	0.204 03	0.803 88
6	0.150 99	0.523 38	0.293 11	0.111 86	0.254 57

Table 3. *Values of the cost functions, agglomeration sizes and number of particles therein, corresponding to tables 1 and 2 after 25 generations*

rank	Π	b^{f}	n^{f}
1	0.677 08	3.2292	33.6732
2	0.790 78	2.0922	9.1581
3	0.796 36	2.0394	8.4821
4	0.799 57	2.0043	8.0517
5	0.800 36	1.9964	7.9568
6	0.806 91	1.9309	7.1991

domain was restricted and rescaled to be centred around the best current parameter set. An average of 11.84 samples per parameter set were needed to meet an ensemble tolerance of TOL = 0.0005 (equation (8.1)). The genetic algorithm was allowed to keep searching for a total of 100 generations, however, *the best set of parameters was obtained in only 25 generations*. The best set of parameters yielded slightly over a tripling of the average agglomerated particle radius, $b^{\mathrm{f}} = b^{*}(1 - \Pi) = 3.23$. This implies that the *average mass* of the remaining particles was approximately 33.67 times greater than those initially, i.e. *on average*, 33.67 original-sized particles were in each remaining particle. Successive frames in a typical flow simulation are shown in figure 5.

9. Concluding remarks

It was the objective of this research to develop a computational framework which assembles very simple models governing vastly different physical phenomena, in order to describe the complex coupled events of agglomeration, particle growth, in thermochemically reacting granular flows. Since modelling of these coupled events is rather complex, and there exists no overall framework available which could be used as a basis, the present work aimed to provide this larger perspective on the problem. Clearly, several components of the model, which were based upon ad hoc assumptions, can be improved. These limitations have been identified in the body of the work. The author is currently collaborating with experimentalists to refine various aspects of the modelling. In particular, experimentally speaking, thermal properties can be a key indicator of the character of a granular flow. For example, in Chung *et al*. (2003), techniques for measuring flow characteristics based upon infrared thermal

velocimetry (ITV) in fluidic microelectromechanical systems (MEMS) were developed. In such an approach infrared lasers are used to generate a short heating pulse in a flowing liquid, and an infrared camera records the radiative images from the heated flowing liquid. The flow properties are obtained from consecutive radiative images. This approach is robust enough to measure granular flows as well. We remark that thermal flow sensors, based on a 'time-of-flight' principle, are also possible (Ashauer *et al*. 1998). In such approaches, a heater generates a short thermal pulse, and a thermal sensor detects the arrival downstream. Such techniques can serve to improve and calibrate the models presented.

Future uses of such particulate flow models may involve (multiscale) coupling to a continuum-type simulation. Specifically, one could *embed such microscale impact simulations into a macroscale continuum simulation*, whereby the macroscale code provides the initial particulate sizes, as well as velocity and thermal distributions, for a point 'box' within the flow, which the microscale granular flow algorithm uses to compute a multibody thermochemical collision analysis for the duration of the (continuum) macroscale time-step. The new microstate variables, i.e. new particulate sizes, velocities, temperatures, etc., are then passed back to the macroscale level, in homogenized form (in terms of fluid continuum parameters) for the macroscale code's next time-step. Theoretical and computational issues related to such multiscale methods for such problems are currently being investigated by the author.

References

Akisanya, A. R., Cocks, A. C. F. & Fleck, N. A. 1997 The yield behavior of metal powders. *Int. J. Mech. Sci.* **39**, 1315–1324.

Anand, L. & Gu, C. 2000 Granular materials: constitutive equations and shear localization. *J. Mech. Phys. Solids* **48**, 1701–1733.

Ashauer, M., Glosch, H., Hedrich, F., Hey, N., Sandmaier, H. & Lang, W. 1998 Thermal flow sensor for liquids and gases. In *Proc. ASME Int. Mechanical Engineering Congress & Exposition, Anaheim, CA*, pp. 427–432. New York: ASME.

Axelsson, O. 1994 *Iterative solution methods*. Cambridge University Press.

Barge, P. & Sommeria, J. 1995 Did planet formation begin inside persistent gaseous vortices? *Astron. Astrophys.* **295**, L1–L4.

Barranco, J. & Marcus, P. 2001 Vortices in protoplanetary disks and the formation of planetesimals. In *Studying Turbulence using Numerical Simulation. Databases-VIII, Center for Turbulence Research, Proc. Summer Program*. Stanford University Press.

Barranco, J., Marcus, P. & Umurhan, O. 2001 Scaling and asymptotics of coherent vortices in protoplanetary disks. In *Studying Turbulence Using Numerical Simulation. Databases-VIII, Center for Turbulence Research, Proc. Summer Program*. Stanford University Press.

Beckwith, S., Henning, T. & Nakagawa, Y. 2000 Dust particles in protoplanetary disks. In *Protostars and planets*, vol. IV (ed. V. Mannings, A. P. Boss & S. S. Russell). Tucson, AZ: University of Arizona Press.

Benz, W. 1994 Impact simulations with fracture. 1. Method and tests. *Icarus* **107**, 98–116.

Benz, W. 2000 From dust to planets. *Spatium* **6**, 3–14.

Blum, J. & Wurm, G. 2000 Impact simulations on sticking, restructuring, and fragmentation of preplanetary dust aggregates. *Icarus* **143**, 138–146.

Brown, S. & Abou-Chedid, G. 1994 Yield behavior of metal powder assemblages. *J. Mech. Phys. Solids* **42**, 383–398.

Chokshi, A., Tielens, A. G. G. M. & Hollenbach, D. 1993 Dust coagulation. *Astrophys. J.* **407**, 806–819.

Chung, J., Grigoropolous, C. & Greif, R. 2003 Infrared thermal velocimetry in MEMS-based fluid devices. *J. MEMS* **12**(3), 365–371.

Cuzzi, J. N., Dobrovolskis, A. R. & Champney, J. M. 1993 Particle-gas dynamics in the midplane of a protoplanetary nebula. *Icarus* **106**, 102–134.

Davis, L. 1991 *Handbook of genetic algorithms*. London: Thompson Computer Press.

Do, I. P. H. & Benson, D. 2001 Micromechanical modeling of shock-induced chemical reactions in multi-material powder mixtures. *Int. J. Plasticity* **17**, 641–668.

Doltsinis, I. St. 1993 Coupled field problems—solution techniques for sequential and parallel processing. In *Solving large-scale problems in mechanics* (ed. M. Papadrakakis). Wiley.

Doltsinis, I. St. 1997 Solution of coupled systems by distinct operators. *Engng Computat.* **14**, 829–868.

Dominik, C. & Tielens, A. G. G. M. 1997 The physics of dust coagulation and the structure of dust aggregates in space. *Astrophys. J.* **480**, 647–673.

Du, Y., Li, H. & Kadanoff, L. P. 1995 Breakdown of hydrodynamics in a one-dimensional system of inelastic particles. *Phys. Rev. Lett.* **74**, 1268–1271.

Fleck, N. A. 1995 On the cold compaction of powders. *J. Mech. Phys. Solids* **43**, 1409–1431.

Goldberg, D. E. 1989 *Genetic algorithms in search, optimization and machine learning*. Addison-Wesley.

Goldberg, D. E. & Deb, K. 2000 Special issue on genetic algorithms. *Computat. Meth. Appl. Mech. Engng* **186**(2–4), 121–124.

Goldsmith, W. 2001 *Impact: the theory and physical behavior of colliding solids*. New York: Dover.

Grazier, K. R., Newman, W. I., Varadi, F., Kaula, W. M. & Hyman, J. M. 1999 Dynamical evolution of planetesimals in the outer solar system. II. The Saturn/Uranus and Uranus/Neptune zones. *Icarus* **140**(2), 353–368.

Grazier, K. R., Newman, W. I., Kaula, W. M. & Hyman, J. M. 2000 Dynamical evolution of planetesimals in the outer solar system. I. The Jupiter/Saturn zone. *Icarus* **140**(2), 341–352.

Gu, C., Kim, M. & Anand, L. 2001 Constitutive equations for metal powders: application to powder forming processes. *Int. J. Plasticity* **17**, 147–209.

Gurson, A. L. 1977 Continuum theory for ductile rupture by void nucleation and growth. Part I. Yield criteria and flow rules for porous media. *J. Engng Mater. Technol.* **99**, 2–15.

Holland, J. H. 1975 *Adaptation in natural and artificial systems*. Ann Arbor, MI: University of Michigan Press.

Johnson, K. 1987 *Contact mechanics*. Cambridge University Press.

Kennedy, J. & Eberhart, R. 2001 *Swarm intelligence*. San Mateo, CA: Morgan Kaufmann.

Kokubo, E. & Ida, S. 1996 On runaway growth of planetesimals. *Icarus* **123**(1), 180–191.

Kokubo, E. & Ida, S. 2000 Formation of protoplanets from planetesimals in the solar nebula. *Icarus* **143**(1), 15–27.

Le Tallec, P. & Mouro, J. 2001 Fluid structure interaction with large structural displacements. *Computat. Meth. Appl. Mech. Engng* **190**(24–25), 3039–3067.

Lewis, R. W. & Schrefler, B. A. 1998 *The finite element method in the static and dynamic deformation and consolidation of porous media*, 2nd edn. Wiley.

Lewis, R. W., Schrefler, B. A. & Simoni, L. 1992 Coupling versus uncoupling in soil consolidation. *Int. J. Numer. Analysis Meth. Geomech.* **15**, 533–548.

Lissauer, J. J. 1993 Planet formation. *A. Rev. Astron. Astrophys.* **31**, 129–174.

Meyers, M. A. 1994 *Dynamic behavior of materials*. Wiley.

Meyers, M. A., Yu, L. H. & Vecchio, K. S. 1994 Shock synthesis in silicides. II. Thermodynamics and kinetics. *Acta Metall. Mater.* **42**(3), 715–729.

Nesterenko, V. F. 2001 *Dynamics of heterogeneous materials*. Springer.

Nesterenko, V. F., Meyers, M. A., Chen, H. C. & LaSalvia, J. C. 1994 Controlled high rate localized shear in porous reactive media. *Appl. Phys. Lett.* **65**(24), 3069–3071.

Onwubiko, C. 2000 *Introduction to engineering design optimization*. Englwood Cliffs, NJ: Prentice Hall.

Pardoen, T. & Hutchinson, J. W. 2000 An extended model for void growth and coalescence. *J. Mech. Phys. Solids* **48**, 2467–2512.

Park, K. C. & Felippa, C. A. 1983 Partitioned analysis of coupled systems. In *Computational methods for transient analysis* (ed. T. Belytschko & T. J. R. Hughes). Amsterdam: North-Holland.

Piperno, S. 1997 Explicit/implicit fluid/structure staggered procedures with a structural predictor and fluid subcycling for 2D inviscid aeroelastic simulations. *Int. J. Numer. Meth. Fluids* **25**, 1207–1226.

Pollack, J. N., Hollenbach, D., Beckwith, S., Simonelli, D. P., Roush, T. & Fong, W. 1994 Composition and radiative properties in molecular clouds and accretion disks. *Astrophys. J.* **421**, 615–639.

Schmidt, L. 1998 *The engineering of chemical reactions*. Oxford University Press.

Schrefler, B. A. 1985 A partitioned solution procedure for geothermal reservoir analysis. *Commun. Appl. Numer. Meth.* **1**, 53–56.

Supulver, K. D. & Lin, D. N. C. 2000 Formation of icy planetesimals in a turbulent solar nebula. *Icarus* **146**(2), 525–540.

Tanga, P., Babiano, A., Dubrulle, B. & Provenzale, A. 1996 Forming planetesimals in vortices. *Icarus* **121**(1), 158–170.

Thadhani, N. N. 1993 Shock-induced chemical reactions and synthesis of materials. *Prog. Mater. Sci.* **37**, 117–226.

Vecchio, K. S. & Meyers, M. A. 1994 Shock synthesis in silicides. I. Experimentation and microstructural evolution. *Acta Metall. Mater.* **42**(3), 701–714.

Weidenschilling, S. J. & Cuzzi, J. N. 1993 Formation of planetesimals in the solar nebula. In *Protostars and planets* (ed. E. H. Levy & J. I. Lunine), vol. III, pp. 1031–1060. Tucson, AZ: University of Arizona Press.

Weidenschilling, S. J., Spaute, D., Davis, D. R., Marzari, F. & Ohtsuki, K. 1997 Accretional evolution of a planetesimal swarm. *Icarus* **128**(2), 429–455.

Wriggers, P. 2002 *Computational contact mechanics*. Wiley.

Wurm, G., Blum, J. & Colwell, J. E. 2001 A new mechanism relevant to the formation of planetesimals in the solar nebula. *Icarus* **151**, 318–321.

Zienkiewicz, O. C. 1984 Coupled problems and their numerical solution. In *Numerical methods in coupled systems* (ed. R. W. Lewis, P. Bettes & E. Hinton), pp. 35–58. Wiley.

Zohdi, T. I. 2002*b* An adaptive-recursive staggering strategy for simulating multifield coupled processes in microheterogeneous solids. *Int. J. Numer. Meth. Engng* **53**, 1511–1532.

Zohdi, T. I. 2003*a* Large-scale statistical inverse computation of inelastic accretion in transient granular flows. *Int. J. Non-Linear Mech.* **8**(38), 1205–1219.

Zohdi, T. I. 2003*b* On the compaction of cohesive hyperelastic granules at finite strains. *Proc. R. Soc. Lond.* A **454**, 1395–1401.

Zohdi, T. I. 2003*c* Genetic design of solids possessing a random-particulate microstructure. *Phil. Trans. R. Soc. Lond.* A **361**, 1021–1043.

Zohdi, T. I. 2003*d* Computational design of swarms. *Int. J. Numer. Meth. Engng* **57**, 2205–2219.

Zohdi, T. I., Monteiro, P. J. M. & Lamour, V. 2002*a* Extraction of elastic moduli from granular compacts. *Int. J. Fracture* **115**, L49–L54.